PAPER

Study on a Doppler-Tolerant Waveform Design for Joint Radar and Communication Systems

Toru TAKAHASHI[†a)], ***Senior Member***, **Yasunori KATO**[†], **Kentaro ISODA**[†], ***and*** **Yusuke KITSUKAWA**[†], ***Members***

SUMMARY In this paper, a Doppler-tolerant waveform is proposed as a transmitting signal for joint radar and communication systems. In the proposed waveform, communication signals are multiplexed at the side band of a linear frequency modulated (LFM) pulse, based on the orthogonal frequency division multiplexing (OFDM) scheme. Therefore, the proposed waveform can maintain Doppler-tolerance in radar use as well as the original LFM pulse can. In addition, it is also capable of flexibly increasing the transmission rate in communication use by assigning more communication signals at the side-band subcarriers. Numerical simulations were carried out to comprehensively examine the proposed waveform in terms of the probability of detection in radar use and the symbol error rate in communication use. In conclusion, the proposed waveform is suited to the transmitting signal for joint radar and communication systems, especially with maintaining Doppler-tolerance to detect fast-moving targets.

key words: *Doppler-tolerance, joint radar and communication system, linear-frequency-modulated pulse, orthogonal frequency-division multiplexing, waveform design*

1. Introduction

Recently, tighter spectrum allocations have become a critical issue in radio wave engineering because of the rapid evolution of various wireless systems, such as mobile communications, wireless sensor networks, wireless power transfer, and radar systems [1], [2]. Various approaches have been proposed with concerning the co-existence and/or the sharing of spectra with wireless communication systems [3], [4]. To the best of the authors' knowledge, three kinds of approaches have addressed this problem thus far. The first mitigates interference from other wireless systems; the second shares the spectrum or waveform between multiple wireless systems; and the third pioneers higher unused frequencies such as millimeter waves and sub-terahertz frequencies. This study focused on a waveform shared between radar and wireless communication systems, which can also be applied to joint radar and communication systems. Especially, we target a Doppler-tolerant waveform by which fast moving targets can be detected in radar use. In addition, we aim to establish a waveform that can flexibly increase the transmission rate in communication use to some extent.

Conventional studies on such shared waveforms can be classified as those based on communication waveforms [6]–[33] and radar waveforms [34]–[60].

Communication-based waveforms are mainly derived from spectrum-spread modulations [6]–[13] or orthogonal frequency-division multiplexing (OFDM) [14]–[30]. In general, both have wide bandwidths and sharp autocorrelation characteristics, which provide high-range resolution and signal processing gain after matched filtering or pulse compression. However, a spectrum-spread modulation is less tolerant of the frequency shift due to the Doppler effect because it corresponds to a phase-modulated pulse waveform in radar [61], [62]. OFDM would also be much less tolerant of the Doppler shift because the ambiguity function of a multi-carrier signal has a single peak in the frequency domain [63]. These communication-based studies have aimed to detect static objects or slow-moving targets such as automobiles, not fast-moving targets such as aircraft. Another communication-based study has proposed a multiple-input and multiple-output radar, where orthogonal phase-shift keying (PSK) signals are transmitted through each branch [31]–[33]. These studies have evaluated their communication performance, but not discussed their radar performance or Doppler tolerance.

On the other hand, most of the radar-based waveforms are pulsed signals for transmitting coded data, which are classified into two kinds of modulations: 1) inter-pulse modulations, that is, pulse-by-pulse modulations, and 2) intra-pulse modulations, wherein communication signals are embedded within a pulsed signal.

Some inter-pulse modulations have employed amplitude-shift keying (ASK) [34], [35], frequency-shift keying (FSK) [36], [37], and PSK [38], [39] for each pulse, as well as digital communication systems do. Pulse-position modulation has also been proposed [40]–[42]. Other inter-pulse modulation schemes employ both up- and down-chirp linear-frequency-modulated (LFM) waveforms to transmit 1-bit data [43], [44]. These inter-pulse modulations could be Doppler-tolerant if the individual pulses were LFM which are well-known Doppler-tolerant pulses due to range-Doppler coupling [61], [62]. However, inter-pulse modulation is not sufficiently flexible to increase the transmission rate of communication messages. In inter-pulse modulation schemes, the transmission rate is determined by the pulse repetition frequency (PRF) and the number of symbols for each pulse. The PRF should be designed on the basis of radar requirements and the number of symbols would be restricted by the signal-to-noise ratio (SNR). Consequently, it

Manuscript received February 27, 2024.
Manuscript revised June 6, 2024.
Manuscript publicized August 30, 2024.
[†]Mitsubishi Electric Corporation, Kamakura-shi, 247-8501 Japan.
a) E-mail: ttoru@ieee.org
DOI: 10.23919/transcom.2024EBP3039

would be difficult for inter-pulse modulation to flexibly increase the transmission rate in joint radar and communication systems.

In intra-pulse modulations, phase-coded waveforms have been frequently employed to transmit coded communication messages [45]–[53]. However, they are much less tolerant of Doppler shifts [61], [62]. Alternative intra-pulse modulations have embedded communication signals within an LFM pulse [54]–[60]. In [54]–[58], the communication signals are embedded using eigenvectors for the correlation matrix of an LFM pulse. Although these studies are analogous to our approach, they do not discuss radar performance or Doppler tolerance. In [59], continuous phase modulations for communication messages are attached to an LFM pulse. The study focuses on the efficiency in terms of the transmitting power and spectrum, but does not discuss the Doppler-tolerance, assuming to detect fast-moving targets such as aircrafts. In our opinion, the waveform in [59] would be less tolerant of Doppler shifts because it is a kind of phase-coded waveforms. In [60], mutually orthogonal sinusoidal phases are added as communication signals to an LFM waveform phase. The embedded communication signals are so subtle that the waveform has successfully maintained the original LFM characteristics as well as Doppler tolerance. However, in return for the radar performance, the bit error rate for communication messages tends to deteriorate. Additionally, the modulation and demodulation schemes are not linear processing, which is a drawback in practice.

To summarize, conventional communication-based waveforms are suitable for higher transmission rates in communication use but are inappropriate for detecting fast-moving targets in radar use. Conversely, conventional radar-based waveforms are suitable for detecting fast-moving targets in radar use, but they have limitations in terms of the transmission rate in communication use. Consequently, there is a trade-off between the transmission rate and the Doppler tolerance.

Therefore, the authors had previously proposed the Doppler-tolerant waveform to minimize the above trade-off to the maximum possible extent [64], [65]. In the proposed waveform, communication symbols were assigned to the subcarrier frequencies within the sideband of an LFM pulse, similar to an OFDM transmission signal. Thus, the proposed waveform could maintain the Doppler tolerance to some extent as well as the original LFM pulse can. In addition, the transmission rate in communication use could be increased by simply assigning more communication symbols to the additional subcarriers. A similar approach is presented in [29], wherein the radar and communication symbols are multiplexed using the OFDM scheme. However, the waveform in [29] is less tolerant of the Doppler shift because the Doppler shift is supposed to be considerably smaller than the subcarrier interval. The waveforms in [54]–[58] may be mathematically equivalent to our proposed waveform because the radar and communication signals are multiplexed inside a waveform using their orthogonality. However, they do not comprehensively discuss and evaluate the radar performance and Doppler tolerance in detail.

The advanced points of this study from our previous studies [64], [65] are:

- Comprehensive examination of the radar performance by the proposed waveform, adding the other conditions
- Theoretical analysis and numerical simulation of the peak-to-average power ratio (PAPR) of the proposed waveform
- Presenting the ambiguity functions in order to clarify how the proposed waveform is Doppler-tolerant
- Proposing a demodulation process to detect embedded communication symbols using an asynchronous receiver
- Comprehensive examination of the communication performance using the proposed demodulation process

The remainder of this paper is organized as follows. Section 2 presents the proposed waveform. Section 3 presents the numerical simulations to validate the proposed waveform.

2. Proposed Waveform Design

2.1 Overview

Figure 1 shows the joint radar and communication system postulated in this study, wherein the radar and the wireless communication are the primary and secondary functions, respectively, with the transmitting signal shared by both. The main beam and sidelobes of the antenna pattern are directed at the radar targets and communication receivers, respectively. The radar must be able to detect fast-moving targets (such as aircraft), with wireless communication transmitting the data associated with radar detection, for instance.

Figure 2 illustrates the concept of the proposed waveform, wherein the radar and communication signals are multiplexed in the frequency domain. A schematic block diagram to generate the proposed waveform is shown in Fig. 3. First, the original LFM pulse is transformed into the frequency domain by fast Fourier transform (FFT), and some subcarrier signals at the sideband of the original LFM

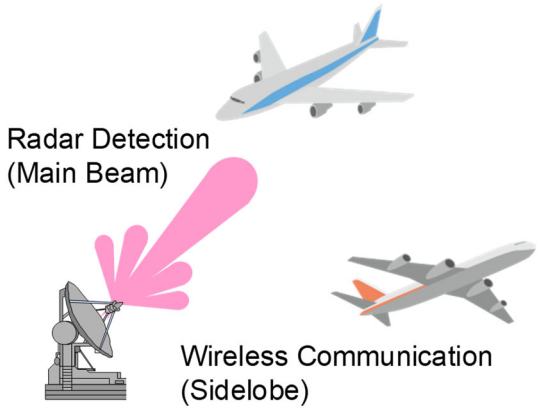

Fig. 1 Joint radar and communication system.

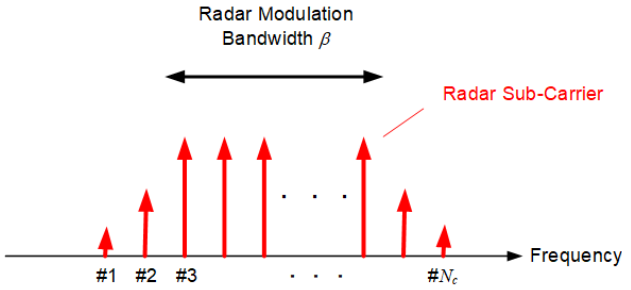

(a) Original LFM pulse spectrum before embedding communication signals.

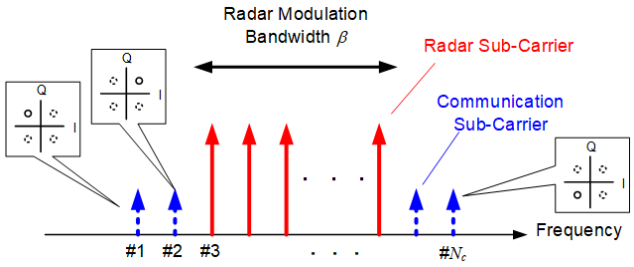

(b) Proposed waveform spectrum after embedding the communication signals.

Fig. 2 Proposed waveform concept in the frequency domain to embed communication signals into an LFM pulse.

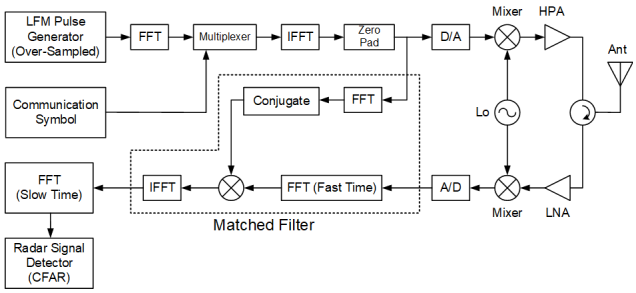

Fig. 3 Block diagram for transmitting and receiving the proposed waveform.

pulse are replaced with complex symbols corresponding to the coded communication messages, as shown in Fig. 2(b). The replaced subcarrier frequencies are outside the modulation bandwidth but within a guard band or regulation band, which are referred to as communication subcarriers. Individual symbols for communication subcarriers are complex values modulated by ASK, PSK, quadrature amplitude modulation, and others. The multiplexed signal is again transformed into the time domain by inverse fast Fourier transform (IFFT) and then formed into a pulsed waveform with pulse width τ and pulse repetition interval *PRI*, as shown in Fig. 4. Note that the envelope of the waveforms varies per pulse because the embedded communication messages also change per pulse.

Figure 3 also includes the receiving diagram to work as a radar, where the receiver is synchronized with the transmitter. In such a synchronized receiver, the signal within the time interval *PRI* is transformed into the frequency domain by FFT and correlated with the reference signal, which should be a replica corresponding to the transmitting pulse (which changes per pulse, as indicated above). Subsequently, the signal is again transformed into the time domain by the IFFT. Although this signal processing is identical to matched filtering or pulse compression in regular radar systems, the reference signal changes per pulse. Doppler processing, which means FFT in the slow-time dimension, follows matched filtering. Finally, the signal or target is detected using a threshold detection scheme, such as a constant false alarm rate (CFAR) detector.

The method to extract embedded communication symbols in asynchronous receivers is described in detail in Sect. 2.6.

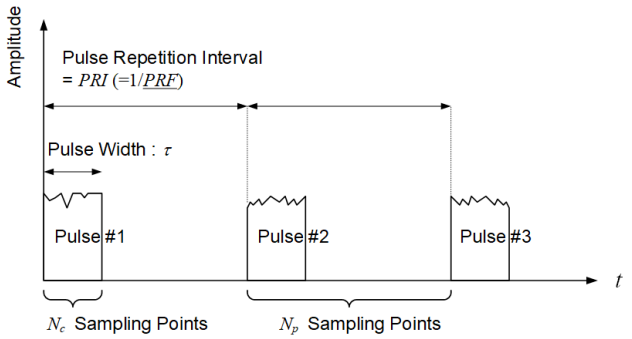

Fig. 4 Proposed waveform schema in the time domain.

2.2 Formulation of the Proposed Waveform

In the time domain, the proposed transmitting waveform can be expressed as:

$$x_{RF}(t) = h\left(\frac{t}{\tau}\right)\sum_{n=0}^{N_c-1} a_n e^{j2\pi(f_c+f_n)t} \tag{1}$$

$$f_n = n\Delta f, \tag{2}$$

where f_c is the carrier frequency (lower bound), f_n is the n-th subcarrier frequency, Δf is the subcarrier frequency interval, a_n is a complex symbol for the n-th subcarrier, and N_c is the total number of subcarriers. The function $h(-)$ is a pulse function given by:

$$h\left(\frac{t}{\tau}\right) = \begin{cases} 1 & 0 \le t \le \tau \\ 0 & otherwise \end{cases}, \tag{3}$$

where τ denotes the pulse width. All component signals in (1) can be orthogonal to each other when, for a given t, Δf is set as:

$$\Delta f = \frac{1}{\tau}. \tag{4}$$

The complex symbol before embedding the communication messages, which is alternatively defined as b_n for the n-th subcarrier, can be derived using the discrete Fourier transform of the original LFM pulse. The original LFM pulse

can be express as:

$$x(t)_{RF} = h\left(\frac{t}{\tau}\right) e^{j2\pi f_c t} e^{j\pi\beta t^2/\tau}, \tag{5}$$

where β is the modulation bandwidth of the original LFM pulse. Therefore, b_n is given by:

$$b_n = \sum_{i=0}^{N_c-1} e^{j\pi\beta(iT_s)^2/\tau} e^{-j2\pi n\Delta f(iT_s)} = \sum_{i=0}^{N_c-1} e^{j\frac{\pi\beta i^2}{f_s N_c}} e^{-j\frac{2\pi i}{N_c}}, \tag{6}$$

where T_s is the sampling interval, and f_s is the sampling frequency, the inverse of T_s. N_c in (6), which is also the number of subcarriers in (1), is the number of samples within the pulse. Note that f_s should be much greater than β to accommodate the communication subcarriers shown in Fig. 2(b), which means that the signal should be oversampled beyond the modulation bandwidth β. In order to lower the oversampling ratio, the subcarrier frequency interval Δf should be narrowed, which means that the pulse width τ should be widened according to (4).

As shown in Fig. 2(b), communication symbols are assigned to the communication subcarriers that are outside the modulation bandwidth β. The number of communication subcarriers is N_{com}. In this study, each communication subcarrier is modulated by M-ary PSK, which can carry k-bit information for $M = 2^k$.

From the above definition, the complex symbol a_n for the n-th subcarrier in (1) can be expressed as:

$$a_n = \begin{cases} b_n & f_n \notin \{f_{com}\} \\ c_n e^{j\frac{2\pi(m-1)}{M}} & f_n \in \{f_{com}\} \end{cases}, \tag{7}$$

where $\{f_{com}\}$ is the communication subcarrier, b_n is given by (6), c_n is the real-valued amplitude of the communication subcarriers, and $m\,(= 1, 2 \ldots, M)$ is the index for M possible phases. In this study, c_n is assumed to be constant across all communication subcarriers and is determined by the fixed ratio η to the average transmitting power of (1) as:

$$c_n^2 = \eta \sum_{n=0}^{N_c-1} |a_n|^2, \tag{8}$$

where the power ratio η should be designed by the communication-link budget. Section 2.7 discusses the design guidelines in detail.

2.3 Maximum Transmission Rate for Communication

In the proposed waveform, M symbols are assigned to each communication subcarrier, which can carry k-bit information for $M = 2^k$. The number of communication subcarriers is N_{com}, as described in Sect. 2.2. Therefore, in theory, the maximum transmission rate R [bps] in communication use is given by:

$$R = k \times PRF \times N_{com}, \tag{9}$$

where PRF is the pulse repetition frequency that equals the inverse of PRI, which should be designed primarily by the radar requirement for the maximum range or velocity of the targets. Therefore, (9) indicates that the proposed waveform has two degrees of freedom, k and N_{com}, to increase the transmission rate. Conversely, conventional interpulse modulations such as [34]–[44], which correspond to $N_{com} = 1$, have only one degree of freedom, that is, k. Thus, the proposed waveform is more advantageous in terms of increasing the transmission rate than conventional ones.

2.4 Received Signal Power to Noise Ratio

The received signal can be expressed as:

$$y_{RF}(t) = \alpha h\left(\frac{t-T}{\tau}\right) \sum_{n=0}^{N_c-1} a_n e^{j2\pi(f_c+f_d+n\Delta f)(t-T)}, \tag{10}$$

where α is a complex propagation factor that includes path loss and target reflectivity. T is the propagation delay time, which is the round-trip time in radar use, or the one-way delay time in communication use. f_d is the Doppler frequency due to the relative speed between the receiver and target.

The average SNR before signal processing can be obtained from (10) as:

$$SNR_{av} = \frac{\frac{1}{\tau}\int_{-\infty}^{\infty} |y_{RF}(t)|^2\, dt}{\sigma_w^2 B} = \frac{P_{r,av}}{\sigma_w^2 B}, \tag{11}$$

where σ_w^2 is the noise power spectral density, B is the receiver bandwidth, and $P_{r,av}$ is the average received power, defined by

$$P_{r,av} \equiv \frac{1}{\tau}\int_{-\infty}^{\infty} |y_{RF}(t)|^2\, dt. \tag{12}$$

Because the received signal due to the proposed waveform is a sum of orthogonal subcarriers, as shown in (10), the average received power can be derived as:

$$P_{r,av} = |\alpha|^2 \sum_{n=0}^{N_c-1} |a_n|^2. \tag{13}$$

If the Doppler shift can be completely compensated via the matched filter, the SNR at the output of the matched filter results in:

$$SNR_{rad} = \frac{\int_{-\infty}^{\infty} |y_{RF}(t)|^2\, dt}{\sigma_w^2} = B\tau SNR_{av} = \frac{\tau|\alpha|^2 \sum_{n=0}^{N_c-1} |a_n|}{\sigma_w^2}. \tag{14}$$

In this study, the SNR defined by (14) is referred to as that of the radar signal, which means that the signal processing gain $B\tau$ is obtained by the matched filter as well as for the regular LFM pulse. Furthermore, (14) indicates the SNR of the radar signal is proportional to the average power within

the pulse. In the original LFM, the average power within a pulse is equal to the peak power because the envelope of the pulse is constant. However, in the proposed waveform, the envelope fluctuates within a pulse, as depicted in Fig. 4, because it is a kind of multi-carrier signals such as OFDM. Therefore, if the transmitting peak power is set equal to that of the original LFM pulse, the SNR (14) can be expressed as:

$$SNR_{rad} = \frac{P_r \tau}{\gamma \sigma_w^2}, \tag{15}$$

where P_r is the received power due to the original LFM pulse, and γ is the PAPR of the proposed waveform. Equation (15) implies that the proposed waveform reduces the SNR of the radar signal in inverse proportion to the PAPR, compared to the original LFM pulse. This is a disadvantage of our waveform over the original LFM pulse and, therefore, the PAPR should be carefully evaluated in the waveform design. The PAPR of the proposed waveform is analyzed in Sect. 2.5 in detail.

Next, the SNR of the communication signals is discussed. As described in Sect. 2.6, the embedded communication symbols, which are assigned to communication subcarriers $\{f_{com}\}$, are extracted after the received signal undergoes FFT in fast time as well as in the OFDM receivers. Therefore, the SNR of the communication signals can be obtained by:

$$SNR_{com} = \frac{\int_{-\infty}^{\infty} |\alpha a_n|^2 \, dt}{\sigma_w^2} = \frac{|\alpha|^2 c_n^2 \tau}{\sigma_w^2}. \tag{16}$$

Equations (14) and (16) yield:

$$SNR_{com} = \eta SNR_{rad} = \eta B \tau SNR_{av}. \tag{17}$$

This indicates that the SNR of the communication signals is proportional to the power ratio η over the SNR of the radar signal.

2.5 Statistical Analysis for Estimating the PAPR

As discussed above, the envelope of the proposed waveform fluctuates within a pulse, depending on the embedded communication symbols, and its PAPR affects the SNR of the radar signal and, as a result, its detection performance. Therefore, the possible PAPR should be evaluated in the waveform design, which can be performed through the following statistical analysis.

Without loss of generality in discussing the PAPR, it can be postulated that the average transmitting power $P_{t,av} = 1$, that is,

$$P_{t,av} = \sum_{n=0}^{N_c-1} |a_n|^2 = 1 \tag{18}$$

Factoring (18), the transmitting baseband signal can be also expressed as:

$$x(t) = Ae^{j\theta(t)} - A \sum_{f_n \in \{f_{com}\}} b_n e^{j2\pi f_n t} + \sum_{f_n \in \{f_{com}\}} c_n e^{j\frac{2\pi(m-1)}{M}} e^{j2\pi f_n t}, \tag{19}$$

where the first term on the right-hand side corresponds to the original LFM pulse with the normalizing amplitude A and phase θ, the second term corresponds to the original subcarrier components with amplitude b_n (which are replaced with communication symbols), and the last term is the communication subcarriers with amplitude c_n. Because c_n is constant across all the communication subcarriers, (19) can be rearranged as:

$$\begin{aligned} x(t) &= e^{j\theta(t)} \left[A - A \sum_{f \in \{f_{com}\}} |b_n| e^{j\phi_n} + c_n \sum_{f_n \in \{f_{com}\}} e^{j\psi_n} \right] \\ &= e^{j\theta(t)} \left[\left\{ A - A \sum_{f_n \in \{f_{com}\}} |b_n| \cos\phi_n + c_n \sum_{f_n \in \{f_{com}\}} \cos\psi_n \right\} \right. \\ &\quad \left. + j \left\{ A \sum_{f_n \in \{f_{com}\}} |b_n| \sin\phi_n + c_n \sum_{f_n \in \{f_{com}\}} \sin\psi_n \right\} \right] \end{aligned} \tag{20}$$

where phases ϕ_n and ψ_n are introduced anew for the second and third terms in (19). Considering that all ϕ_n and ψ_n can be assumed to be random and uncorrelated with each other, the real and imaginary parts of (20) asymptotically become Gaussian random variables according to the central limit theorem. The means of the real and imaginary parts of (20) are A and 0, respectively, and the variance of each is given by:

$$\sigma^2 = \frac{1}{2} c_n^2 N_{com} + \frac{1}{2} A^2 \sum_{f_n \in \{f_{com}\}} |b_n|^2 = \frac{1}{2} \eta N_{com} + \frac{1}{2} A^2 \sum_{f_n \in \{f_{com}\}} |b_n|^2 . \tag{21}$$

Thus, the signal power, $\chi = |x(t)|^2 > 0$, becomes a non-central chi-square random variable with 0-th degrees of freedom [66], and the probability density function is given by:

$$p(\chi) = \frac{1}{2\sigma^2} e^{-\frac{A^2+\chi}{2\sigma^2}} I_0\left(\frac{A\sqrt{\chi}}{\sigma^2} \right), \tag{22}$$

where $I_0(-)$ is a modified Bessel function of the order of 0. The average transmitting power $P_{t,av}$ in a pulse can be approximated as the expectation of χ, which is given by:

$$E[\chi] = 2\sigma^2 + A^2 \approx P_{t,av} = 1. \tag{23}$$

Substituting (21) into (23) yields:

$$A^2 = \frac{1 - \eta N_{com}}{1 + \sum_{f_n \in \{f_{com}\}} \left| b_n^2 \right|}. \tag{24}$$

According to (24), the parameter A, which corresponds to the amplitude of the original LFM pulse, can be obtained from the average power of the communication subcarriers before and after being replaced with communication symbols.

From (22), the probability for $\chi < \chi_p$ can be given by:

$$P\left[\chi < \chi_p\right] = \int_0^{\chi_p} p(\chi)d\chi = 1 - Q_1\left(\frac{A}{\sigma}, \frac{\sqrt{\chi_p}}{\sigma}\right), \quad (25)$$

where $Q_1(-)$ is the Marcum Q function, which is defined by:

$$Q_1(\alpha, \gamma) = \int_\gamma^\infty t \exp\left[-\frac{1}{2}\left(t^2 + \alpha^2\right)\right] I_0(\alpha t)dt. \quad (26)$$

Equation (26) provides the probability of $\chi < \chi_p$ at a sampling point within a pulse. Therefore, the probability for $\chi < \chi_p$ at all sampling points within a pulse becomes:

$$P\left[\chi < \chi_p; 0 \le t \le \tau\right] = \left\{1 - Q_1\left(\frac{A}{\sigma}, \frac{\sqrt{\chi_p}}{\sigma}\right)\right\}^{N_c}. \quad (27)$$

Because $P_{t,av} = 1$, (27) corresponds to the cumulative probability distribution (CDF) of the PAPR. Referring to the PAPR as γ, the CDF of the PAPR can be rearranged as:

$$F(\gamma) = \left\{1 - Q_1\left(\frac{A}{\sigma}, \frac{\sqrt{\gamma}}{\sigma}\right)\right\}^{N_c}. \quad (28)$$

Because (28) includes the Marcum Q function, it is convenient to derive a simplified formula. According to Appendix A, the upper bound for the CDF of the PAPR can be approximated as:

$$F(\gamma) = \left\{1 - \frac{\sigma}{\sqrt{2\pi}\left(\sqrt{\gamma} - A\right)} e^{-\frac{(\sqrt{\gamma}-A)^2}{2\sigma^2}}\right\}^{N_c}. \quad (29)$$

2.6 Demodulation of Communication Messages in Asynchronous Receivers

Figure 3 also shows the demodulation process to detect radar signals, but this does not apply to the demodulation of communication symbols because, in general wireless communication, the receiver is usually not synchronized with the transmitter. In addition, in order to accurately detect the communication symbols assigned to communication subcarriers, it is necessary to compensate for the Doppler frequency and phase shift that are added through the propagation path. Herein, a demodulation process is proposed for detecting communication symbols using an asynchronous receiver.

Figure 5 shows a block diagram of the proposed demodulation process, assuming the following conditions:

- Specification of the original LFM pulse is known at the receiver.
- The subcarrier frequencies at which the communication symbols are assigned are known at the receiver.
- The distance between the transmitter and receiver is unknown and shall be estimated at the receiver.
- The Doppler frequency and phase shift through the propagation path are unknown and shall be estimated at the receiver.
- Time is not synchronized between the transmitter and receiver.
- The sampling frequency is approximately synchronized between the transmitter and receiver.
- The propagation channel is not dependent on the frequency.

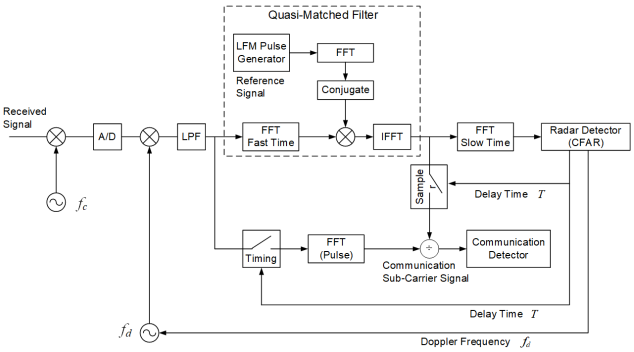

Fig. 5 Block diagram for the demodulation of communication symbols in an asynchronous receiver.

A feature of the proposed demodulation is to apply radar signal processing to estimate the Doppler frequency and delay time between the transmitter and the receiver, which results in an accurate estimation, as discussed in Appendices B and C. The theory of the proposed demodulation is described below.

Initially, consider that the original LFM pulse is transmitted, which can be expressed in the baseband as:

$$x(t) = h\left(\frac{t}{\tau}\right) e^{j\pi\beta t^2/\tau}. \quad (30)$$

The received signal corresponding to (30) can be expressed in the baseband as:

$$y(t) = \alpha h\left(\frac{t-T}{\tau}\right) e^{-j2\pi f_c T} e^{j2\pi f_d(t-T)} e^{j\pi\beta(t-T)^2/\tau}, \quad (31)$$

where α is a complex propagation factor that includes path loss. T is the propagation delay time between the transmitter and receiver. f_d is the Doppler frequency due to the relative speed between the transmitter and receiver. Note that t and T in (31) are estimated by the receiver clock, which is not necessarily synchronized with that of the transmitter.

In the proposed demodulation process, as shown in Fig. 5, the original LFM pulse is employed as the reference signal of matched filtering Therefore, the output signal after matched filtering can be expressed as:

$$z(t) = \alpha e^{-j2\pi f_c T} e^{j\pi f_d(t-T)} e^{j\pi\beta(r-T)} \times \tau\left\{1 - \frac{|t-T|}{\tau}\right\} \frac{\sin\left[\pi\left\{f_d\tau + \beta(t-T)\right\}\left\{1 - \frac{|t-T|}{\tau}\right\}\right]}{\pi\left\{f_d\tau + \beta(t-T)\right\}\left\{1 - \frac{|t-T|}{\tau}\right\}}. \quad (32)$$

As shown in Fig. 5, T and f_d are estimated after performing

the matched filter, Doppler signal processing (FFT) in slow time, and CFAR detection. If the Doppler frequency is completely compensated by the estimated f_d, the output signal after the matched filtering at T becomes:

$$z(T) = \alpha\tau e^{-j2\pi f_c T}. \tag{33}$$

This implies that the signal after ideal matched filtering involves all the effects (added through the propagation path) of the transmitting signal. However, this feature is not preserved when transmitting our proposed signal (in which communication symbols are embedded) because every transmitting signal is different from the reference signal and, consequently, the matched filter is not ideal in reality. Hence, such signal processing has been referred to as a "quasi-matched filter" in Fig. 5. However, it can be assumed that the feature of (33) will be maintained to some extent because the communication subcarriers are outside the modulation bandwidth β which is a significant part of the original LFM pulse, and their power would be minor enough if bt of the original LFM pulse is sufficiently large [61]. Nevertheless, the deviation from the ideal output (33) should be evaluated in advance. Section 3.8 examines the deviation in detail through numerical simulations.

In addition, the quasi-matched filter output fluctuates per pulse, depending on the embedded communication symbols. This may degrade the Doppler signal processing for estimating the Doppler frequency, which should also be evaluated in advance. Section 3.8 also examines the Doppler signal processing in detail through numerical simulations.

Next, we discuss how to extract the communication symbols using the matched filter output (33) with the assumption that the "quasi-matched filter" is approximately ideal. The received signal due to our proposed waveform is given by (10) and the baseband signal after compensating for the Doppler frequency can be expressed as:

$$y(t) = \alpha e^{-j2\pi T} h\left(\frac{t-T}{\tau}\right) \sum_{n=0}^{N_c-1} a_n e^{j2\pi f_n (t-T)}. \tag{34}$$

As shown in Fig. 5, the proposed demodulation process performs a Fourier transform on (34) at $t = T$ and divides its output by (33), which yields:

$$\frac{1}{z(T)} \int_{-\infty}^{\infty} y(t) e^{-j2\pi f_{n'}(t-T)} dt = \frac{a_{n'}}{\tau}. \tag{35}$$

Finally, a complex symbol $a_{n'}$ at frequency $f_{n'}$ can be obtained. If $f_{n'}$ is a communication subcarrier, then a communication symbol can be extracted.

2.7 Design Guideline for Communication Subcarrier Power

The parameter η in (8) should be determined, based on the link budgets for both radar and communication systems.

The link budget for a radar system is derived using the radar equation [62], and the received power is given by:

$$P_{r,rad} = \frac{P_t G_{t,rad} G_{r,rad} \sigma \lambda_c^2}{(4\pi)^3 R^4}, \tag{36}$$

where P_t is the transmitting power, $G_{t,rad}$ and $G_{r,rad}$ are the transmitting and receiving antenna gains, respectively, in the target direction, R is the distance from the transmitter to the target, σ is the radar cross section (RCS) of the target, and λ_c is the wavelength at the carrier frequency f_c.

On the other hand, the link budget for a wireless communication system is derived by using the Friis transmission formula [62], and the received power is given by:

$$P_{r,com} = \frac{P_t G_{t,com} G_{r,com} \lambda_c^2}{(4\pi R)^2}, \tag{37}$$

where $G_{t,com}$ is the transmitting antenna gain in the receiver direction which may differ from that of the radar target. $G_{r,com}$ is the receiving antenna gain. R in (37) is the distance from the transmitter to the communication receiver. It is assumed in (36) and (37) that the maximum range (distance) in radar use is the same as that in communication use.

In the proposed waveform, the SNR of the radar signal is related to that of the communication signals with (8). If the power ratio η is designed as:

$$\eta_b = \frac{G_{t,rad} G_{r,rad} \sigma}{4\pi R^2 G_{t,com} G_{r,com}}, \tag{38}$$

both SNRs would be equal. Generally speaking, the SNR required for radar is not necessarily equal to that required for wireless communication. The SNR required for radar depends on the false alarm rate (P_{FA}) and probability of detection (P_D), and the SNR required for wireless communication depends on the accepted symbol error rate (SER). For example, the SNR required for radar in Swerling case 0 is 10.4 dB for typical $P_D = 0.5$ and $P_{FA} = 10^{-5}$. On the other hand, the SNR required for wireless communication in BPSK modulation is 9.6 dB for typical SER $= 10^{-5}$. These SNRs are not so different from each other. That means that (38) can provide a guideline for the required power ratio η.

Figure 6 shows a typical example of η given by (38). In

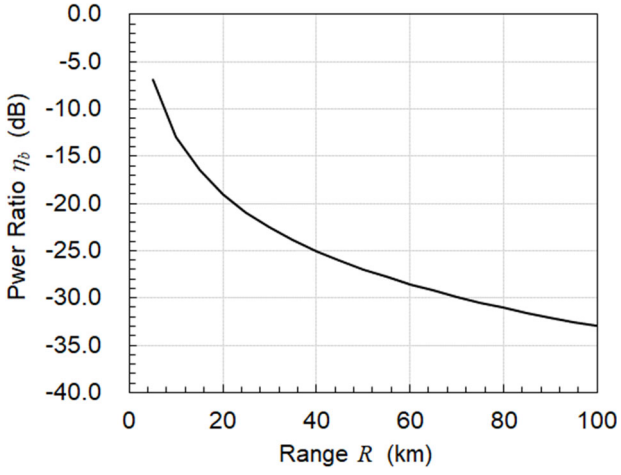

Fig. 6 Typical example of the required power ratio η.

this case, the transmitting/receiving antenna for radar is supposed to be a high-gain antenna with gain $G_{t,rad} = G_{r,rad} =$ 35 dBi. The target RCS is assumed to be 20 m^2, which corresponds to that of medium-sized jet aircraft. The communication receivers are assumed to be located across the sidelobes of the transmitting antenna pattern with gain of $G_{t,com} = 5$ dBi, which corresponds to a relative sidelobe level of −30 dB. The receiving antennas of the communication receivers are assumed to be omnidirectional antennas with gain of $G_{r,com} = 0$ dBi.

According to Fig. 6, at long range, the required power ratio η becomes quite low. Therefore, in general, the power ratio η would be small enough. In the numerical simulations in the next section, it is postulated that $\eta = -14$, −20, and −26 dB.

3. Numerical Simulations

Numerical simulations of signal detection were performed to examine the proposed waveform for both radar and communication usage.

3.1 Simulation Conditions

Table 1 lists the simulation conditions. Every parameter in Table 1 is normalized by the sampling time T_s or the sampling frequency f_s. In the following studies, all results are represented with these normalized parameters. However, for better understanding, numerical examples are also added to Table 1. It can be seen that the simulations have assumed quite large Doppler frequency, that is, fast-moving targets.

In the simulations, random bit sequences were generated as communication messages, and coded symbols were assigned to the communication subcarriers of each transmitting waveform. The radar signals were detected through the cell-averaging CFAR (CA-CFAR) process in the range domain after matched filtering. The FFT in slow time was not included in the simulations to examine the intrinsic characteristics of the proposed waveform. The communication signals were detected based on the demodulation process described in Sect. 2.6.

3.2 Embedding Communication Symbols

Figure 7 shows the transmitted signal spectra before and after embedding the communication symbols. In the figure, the abscissa represents the frequency normalized by the subcarrier interval Δf. The frequency band from 0 to 16 Δf corresponds to the modulation bandwidth β. The number of communication subcarriers in this case is four, and communication symbols are assigned at both sidebands of the modulation, that is, 17 Δf, 18 Δf, 30 Δf, and 31 Δf, factoring frequency aliasing. In addition, the peak amplitude of each signal is normalized to 1, that is, 0 dB in the time domain, as shown in Sect. 3.3.

Table 1 Simulation conditions.

Items	Value	Example
Carrier Frequency f_c	f_c	10 GHz
Sampling Interval T_s	T_s	1 μs
Sampling Frequency f_s	$1 / T_s$ (= f_s)	1 MHz
Pulse Width τ	32 T_s	32 μs
Modulation Bandwidth of the original LFM β	0.5 f_s	0.5 MHz
Pulse Repetition Interval *PRI*	256 T_s	256 μs
Subcarrier Interval Δf	0.03125 f_s	31.25 kHz
Number of All Subcarriers N_c	32	32
Number of Subcarriers within the modulation bandwidth β	17	17
Number of Communication Subcarriers N_{com}	4	4
Modulation Method for Communication	BPSK	BPSK
Power Ratio for Communication Subcarriers η	–14 dB or –20 dB or –26 dB	–14 dB or –20 dB or –26 dB
Delay Time of the received signal T	100 T_s	100 μs (= 30 km)
Doppler Frequency of the received signal f_d	0.0 0.1f_s (= 3.2 Δf)	0.0 (static) 100 kHz (1500 m/s)
RCS Fluctuation of the target	Swerling case 0	Swerling case 0
Propagation Channel	AWGN	AWGN
False Alarm Rate for Radar Detection	10^{-5}	10^{-5}
Number of Reference Cells for CA-CFAR	251	251
Number of Guard Cells for CA-CFAR	2 at both sides	2 at both sides

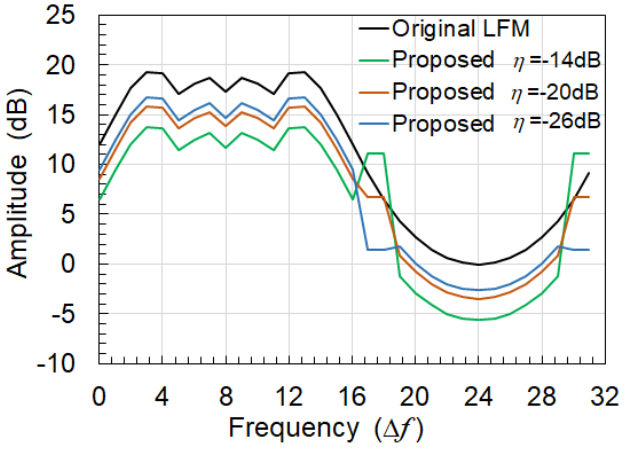

Fig. 7 Transmitting signal spectra before and after embedding communication symbols.

3.3 Transmitting Signals in the Time Domain

Figures 8(a), (b), and (c) show the envelopes of the transmitting signals in the time domain, which correspond to all combinations of the communication symbols, the number of which is $2^4 = 16$ for BPSK. In the figures, the abscissa is the time normalized by the sampling interval T_s and the ordinate is the amplitude normalized by the maximum am-

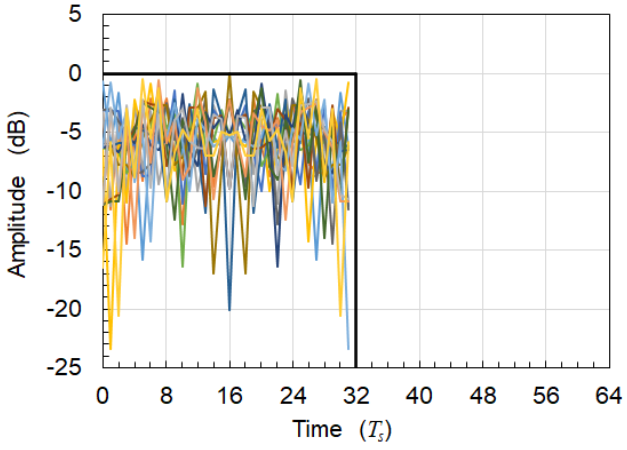

(a) η = -14dB

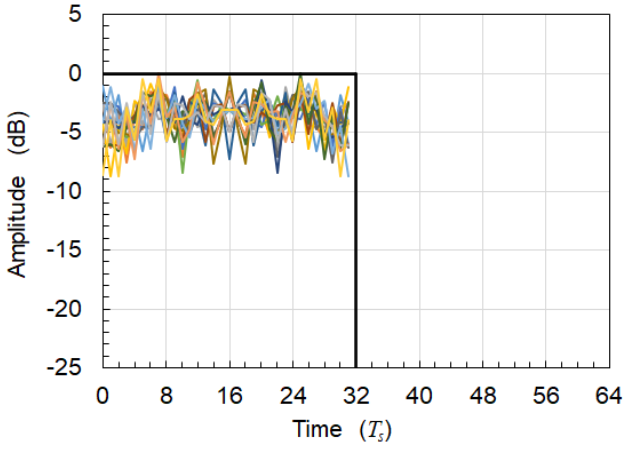

(b) η = -20dB

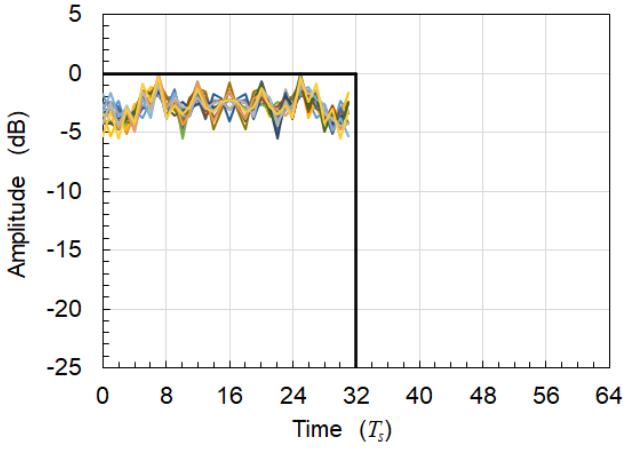

(c) η = -26dB

Fig. 8 Envelope of the transmitting signal in the time domain.

plitude among all signals.

In addition, the envelope of the original LFM pulse is depicted by a bold black line.

As shown in Fig. 8, the envelopes of the proposed waveform fluctuate within the pulse, and the PAPR increases as the power ratio η; that is, the communication subcarrier power becomes large, as discussed in Sect. 2.4.

3.4 PAPR Distribution

Figures 9(a), (b), and (c) show the CDFs of the PAPR in the transmitting signals compared with the theoretical predictions. Each communication subcarrier is modulated by BPSK or QPSK in these simulations. The theoretical predictions are provided by (28) and (29), which, respectively, are referred to as "Theory" and "Approximate Theory" in the figures.

It is interesting that, according to Fig. 9, the CDF is not greatly dependent on modulation schemes (BPSK/QPSK) even though QPSK is more random in terms of phase than BPSK. These numerical results imply that the phases ϕ_n and ψ_n in (20) are approximately random regardless of the modulation schemes for communication subcarriers, as assumed in Sect. 2.5. This is because these phases consist of multiple factors, such as the PSK, LFM, and subcarrier phases, which cause their randomness.

In addition, the numerical results were in good agreement with the theoretical predictions based on (28) or (29). In conclusion, these theories can be employed to estimate the PAPR in the proposed waveform.

3.5 Ambiguity Functions

The ambiguity function of the proposed waveform can be defined as an LFM pulse [61], which is given by:

$$\hat{A}(t, f_d) \equiv \int_{-\infty}^{\infty} x(s) e^{j2\pi f_d s} x*(s-t) ds. \tag{39}$$

Actually, because the proposed waveform is a multi-carrier signal expressed by (1), the integral in (39) should be replaced with the summation.

The ambiguity function of the original LFM pulse before embedding the communication symbols is illustrated in Fig. 10. In the figure, the abscissa is the Doppler mismatch normalized by the subcarrier interval Δf, and the ordinate is the delay time normalized by the pulse width τ. The contour map is normalized and depicted in dB. As shown in Fig. 10, the ambiguity function of the LFM pulse is skewed, which is well known as range-Doppler coupling, leading to the Doppler tolerance of the LFM pulse.

Figures 11(a), (b), and (c) show the ambiguity functions of the proposed waveform. In the proposed waveform, the ambiguity function is not uniquely determined because it depends on the embedded communication symbols. Therefore, each image in Fig. 11 is a typical ambiguity function corresponding to the waveform with the maximum PAPR in Fig. 8. Nevertheless, as can be seen, every ambiguity function is skewed as well as the original LFM pulse, and the range-Doppler coupling is also maintained to some extent.

However, the amplitude tends to decrease in comparison with the original LFM pulse as the Doppler mismatch

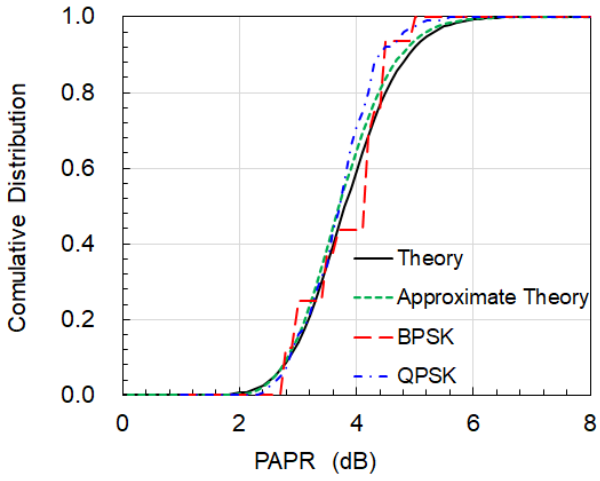

(a) η = -14dB

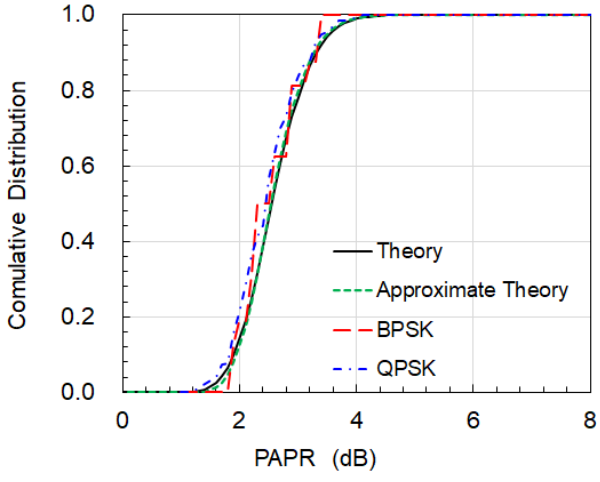

(b) η = -20dB

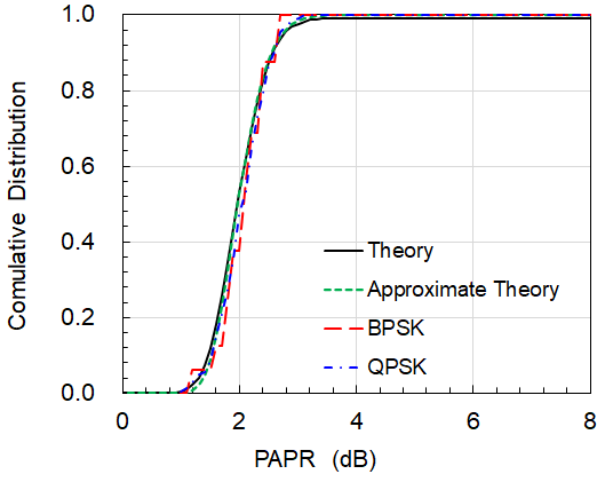

(c) η = -26dB

Fig. 9 CDF of the PAPR in the proposed waveform.

or communication subcarrier power increases. This would reduce the probability of detection. The probability of radar signal detection is examined in Sects. 3.6 and 3.7. In addition, the sidelobe characteristic deteriorates as the communication subcarrier power increases. Reducing the sidelobes will be focused on in future work.

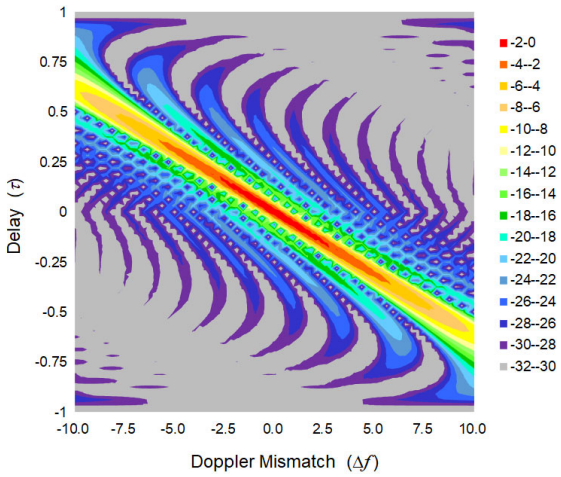

Fig. 10 Ambiguity function of the original LFM pulse.

Table 2 Average SNR for P_D = 0.5 (Static targets, f_d = 0).

Power Ratio η (dB)	Proposed waveform (dB)	LFM pulse (dB)	Difference (dB)
–14	–4.59	–4.64	0.05
–20	–4.64	–4.64	0.00
–26	–4.63	–4.64	0.01

3.6 Radar Signal Detection Performance for Static Targets

Figure 12 shows the probability of radar signal detection for static targets by CA-CFAR process in the range domain. In the figure, the abscissa represents the average SNR before matched filtering. The probability of detection due to the original LFM pulse is also plotted for reference, which is theoretically given for Swerling case 0 by [61]:

$$P_D = Q_1\left(\sqrt{2SNR_{rad}}, \sqrt{-2\ln P_{FA}}\right), \tag{40}$$

where $Q_1(-)$ is the Marcum Q function defined by (26), SNR_{rad} is the SNR for the radar signal given by (14), P_{FA} is the false alarm rate. The SNRs required for P_D = 0.5 are summarized in Table 2. According to the figure and table, the numerical results were in good agreement with those of the original LFM. However, the average SNR of the proposed waveform is not necessarily equal to that of the original LFM pulse, as discussed in Sect. 2.4. If the transmitting peak power is set to equal that of the original LFM pulse, the SNR of the proposed waveform would be reduced according to (15).

3.7 Radar Signal Detection Performance for Fast-Moving Targets

When there is a Doppler mismatch corresponding to a moving target, the peak of the matched filter output will be

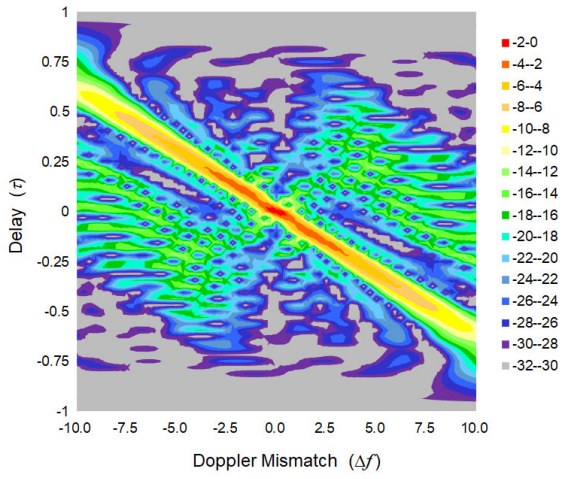

(a) η = -14dB

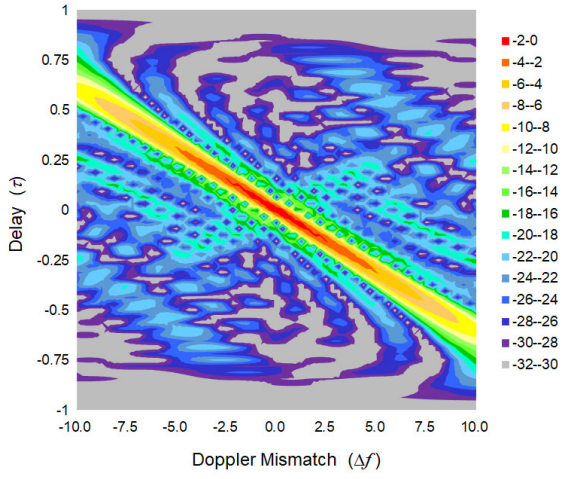

(b) η = -20dB

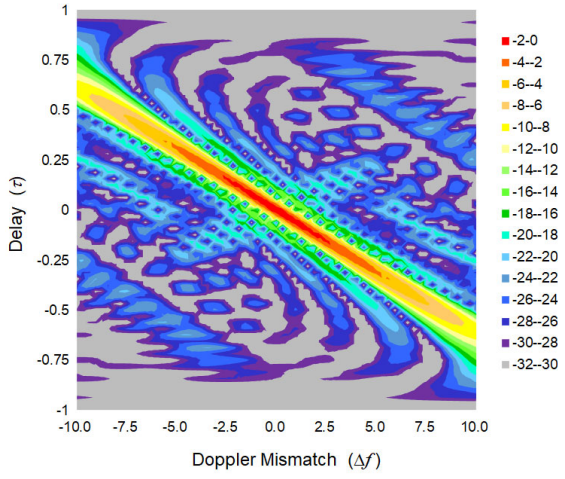

(c) η = -26dB

Fig. 11 Typical ambiguity functions of the proposed waveform.

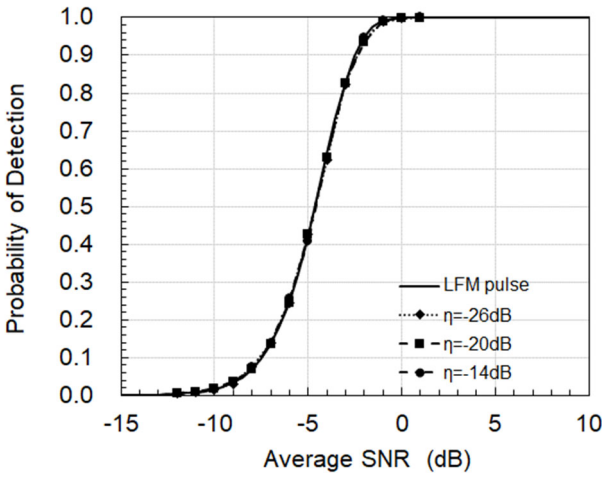

Fig. 12 Probability of radar signal detection for static targets.

shifted in the time dimension due to the range-Doppler coupling, as shown in Fig. 11, the time shift of which is theoretically predicted by [61]:

$$t = -\frac{\tau f_d}{\beta}. \tag{41}$$

Thus, the probability of detection was evaluated at the shifted time in both the theory and numerical simulations. In theory, the SNR at the shifted time is reduced to:

$$SNR'_{rad} = \left(1 - \left|\frac{f_d}{\beta}\right|\right) SNR_{rad} \tag{42}$$

Thus, the probability of detection due to the original LFM pulse must be evaluated with factoring (42).

Figure 13 shows the probability of radar signal detection for fast-moving targets with a Doppler frequency of $0.1 f_s$. Note that this Doppler frequency is equal to 3.2 Δf, that is, beyond the subcarrier interval. From Fig. 13, the SNR required for P_D = 0.5 is also summarized in Table 3.

According to Fig. 13 and Table 3, the proposed waveform requires a slightly higher SNR than the original LFM pulse when detecting fast-moving targets. In addition, the probability of detection is reduced as the power ratio η, i.e., the communication subcarrier power increases. However, the performance degradation is not so severe that the signals can be detected to some extent. This means that the proposed waveform has Doppler tolerance as well as the original LFM pulse does. In practice, it is important to design the minimum power ratio η required for communication systems, the guidelines of which have been discussed in Sect. 2.7. In our opinion, because the power ratio η is small enough according to Sect. 2.7 the proposed waveform could be sufficiently Doppler-tolerant to detect fast moving targets as well as the LFM pulse can.

Next, the proposed waveform is compared in terms of the Doppler-tolerance to a conventional LFM-based waveform [59], that is, phase-attached radar/communication (PARC) waveform. In [59], continuous phase modulations

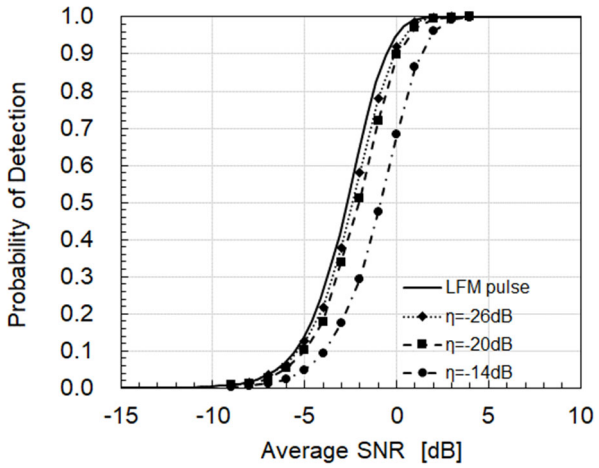

Fig. 13 Probability of radar signal detection for fast-moving targets with $f_d = 0.1 f_s$ ($= 3.2\Delta f$).

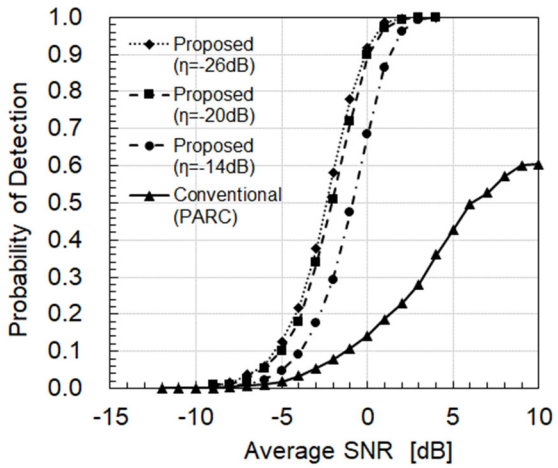

Fig. 14 Comparison of the probability of radar signal detection using the PARC and proposed waveforms for fast-moving targets with $f_d = 0.1 f_s$.

Table 3 Average SNR for $P_D = 0.5$ (Fast-moving targets, $f_d = 0.1 f_s$).

Power Ratio η (dB)	Proposed Waveform (dB)	LFM pulse (dB)	Difference (dB)
–14	–0.87	–2.70	1.82
–20	–2.06	–2.70	0.64
–26	–2.40	–2.70	0.03

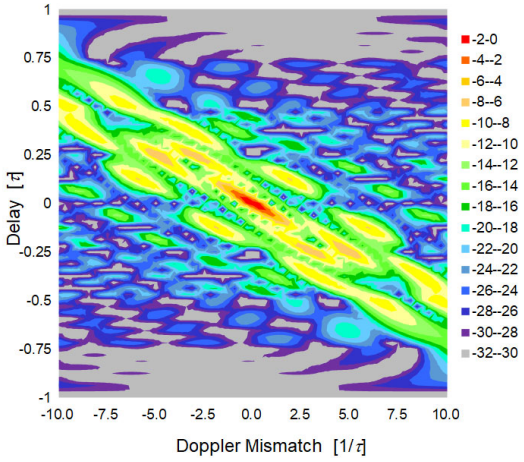

Fig. 15 Typical ambiguity function of the PARC waveform.

for communication messages are attached to an LFM pulse.

Figure 14 shows the probability of radar signal detection using the PARC and proposed waveforms, wherein fast-moving targets with a Doppler frequency of $0.1 f_s$ are assumed to be detected. In the PARC waveform, 4 BPSK modulations were attached to the original LFM pulse, which is equal to the transmission rate in this study and corresponds to the modulation index $h = 1$ in [59]. In the case of the PARC waveform, the maximum probability of radar signal detection is approximately 0.6 and the fast-moving targets could not be detected exactly even if the SNR is so high. The reason why the PARC waveform is so less Doppler-tolerant is because it loses the range-Doppler coupling. Figure 15 shows a typical ambiguity function of the PARC waveform. Compared with the ambiguity functions of the proposed waveform shown in Fig. 11, the range-Doppler coupling is not apparently maintained in the PARC waveform. The range-Doppler coupling is due to the quadratic phase distribution of the original LFM pulse. However, adding some phase modulation within the LFM pulse like the PARC waveform deviates the resultant phase distribution from the quadratic one, which results in losing the range-Doppler coupling. On the other hand, in the proposed waveform, the range-Doppler coupling is maintained to some extent. In conclusion, the proposed waveform is more Doppler-tolerant than the PARC waveform.

3.8 Radar Signal Detection in Asynchronous Receivers

As discussed in Sect. 2.6, the quasi-matched filter in the asynchronous receivers is not ideal. Consequently, its output slightly fluctuates pulse by pulse depending on the embedded communication symbols, which may deteriorate not only the communication signal detection via (35) but also the radar signal detection which estimates the delay time T and the Doppler frequency f_d to be compensated. Therefore, this section examines the performance of radar signal detection in detail before demonstrating the detection of the communication signal.

Figures 16(a) and (b) show the CDFs of the output deviations due to the quasi-matched filter in terms of the amplitude and phase, respectively. In the figures, the abscissa represents the amplitude or phase deviation from the ideal matched-filter output. In the simulations, a Doppler frequency of $1.6\,\Delta f$ is assumed for the received signals, which corresponds to half of the radar target listed in Table 1. According to Figs. 16(a) and (b), the amplitude and phase deviations tend to increase as the power ratio η, that is, the communication subcarrier power, increases. However, the maximum amplitude and phase deviations from the ideal

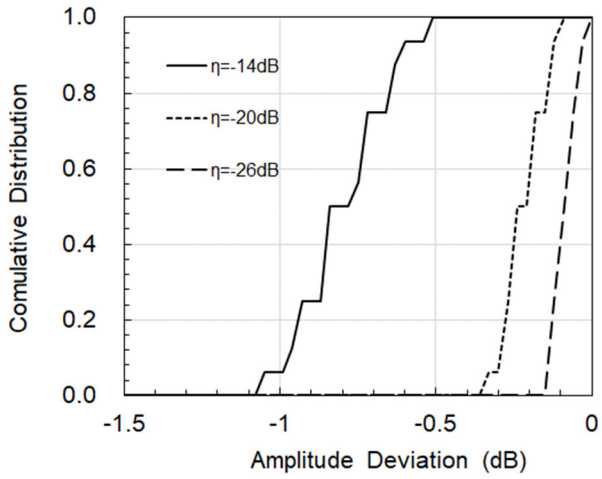

(a) Amplitude deviation.

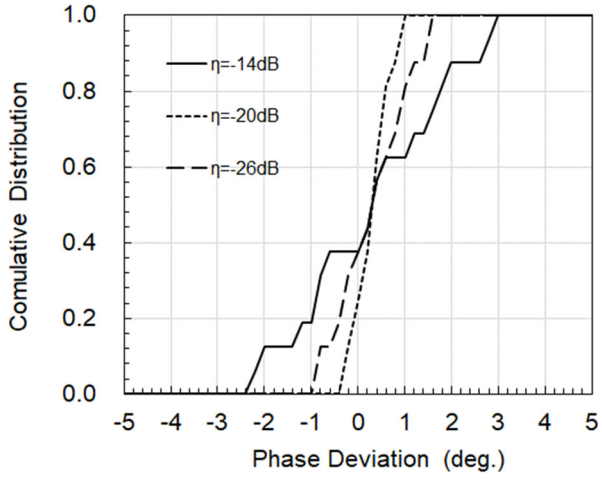

(b) Phase deviation.

Fig. 16 CDF of the quasi-matched filter output deviation.

matched filter output are 1.1 dB and 3.0 deg. respectively. Since these deviations are quite small in comparison with the amplitude and phase variations due to the modulation for each communication subcarrier, they would not so affect communication signal detection. In other words, each communication symbol can be approximately detected using (35), which is confirmed in Sect. 3.9.

The deviation ranges of the quasi-matched filter output are 0.51 dB in amplitude and 5 deg. in phase. Even though such deviation ranges are unlikely to seriously affect the subsequent Doppler processing, its performance is examined in detail.

Figure 17 shows the Doppler spectrum after FFT in slow time. In the simulation, a Doppler frequency of 1.6 Δf was again assumed for the received signals, and the number of received pulses in the slow time was 64. To precisely evaluate our proposed scheme, the receiving noise was not considered. The abscissa of Fig. 17 is the Doppler frequency normalized by the frequency resolution, which is given by:

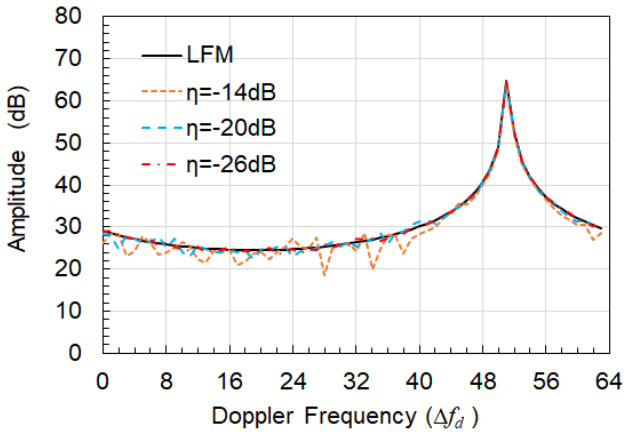

Fig. 17 Doppler spectrum after FFT in slow time.

$$\Delta f_d = \frac{PRF}{N_p}, \tag{43}$$

where PRF is the pulse repetition frequency that equals the inverse of PRI listed in Table 1 and N_p is the number of received pulses in the slow time. Note that the assumed Doppler frequency is much greater than the PRF and, therefore, Fig. 17 depicts the ambiguous response of the assumed Doppler frequency.

As shown in Fig. 17, the frequency response is good enough to estimate the Doppler frequency as well as with the original LFM pulse, even though the sidelobe characteristics fluctuate slightly.

3.9 Performance of Communication Signal Detection in Asynchronous Receivers

Figures 18(a), (b), and (c) show the SERs obtained through the proposed demodulation process. The abscissa in each figure represents the average SNR before FFT. The theoretical predictions of the SER for BPSK in an AWGN channel are also plotted for reference, which is given by [66]:

$$P_e = Q\left(\sqrt{2SNR_{com}}\right), \tag{44}$$

where SNR_{com} is the SNR of the communication signals given by (17) and $Q(-)$ is the Q function, which is defined by:

$$Q(x) = \frac{1}{\sqrt{2\pi}} \int_x^\infty e^{-\frac{t^2}{2}} dt. \tag{45}$$

As these figures show, the simulation results are in good agreement with the theoretical predictions for a higher SNR, but not for a lower SNR, especially for an average SNR $<$ 0 dB. This is because the quasi-matched filter output involves significant noise in the case of a lower SNR and, as a result, it cannot exactly estimate the propagation channel (33) to be compensated. Consequently, the complex symbol for each communication subcarrier cannot be estimated at all via (35) regardless of the power ratio η, as shown in Figs. 18(a) to 18(c). Nevertheless, it can be concluded that

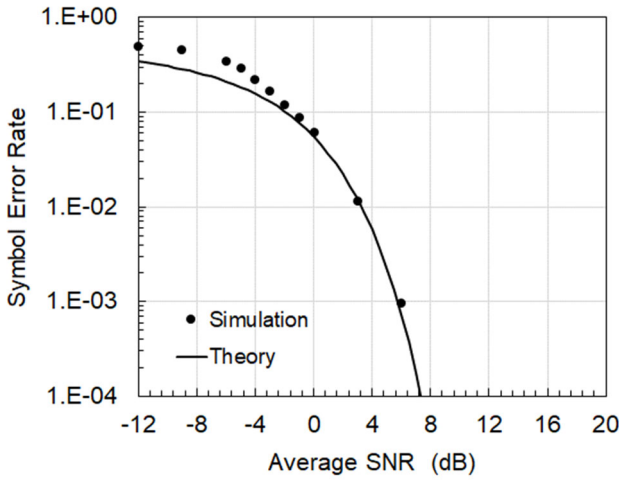

(a) η = -14dB

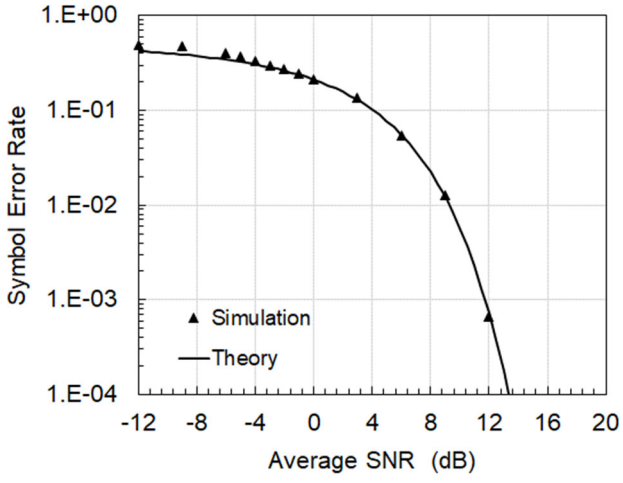

(b) η = -20dB

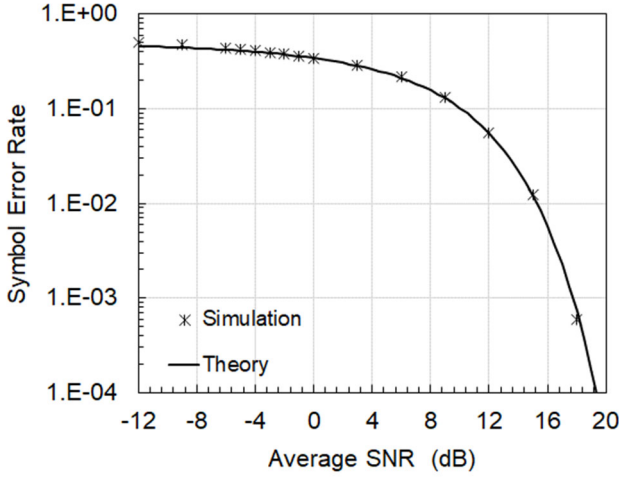

(c) η = -26dB

Fig. 18 Doppler spectrum after FFT in slow time.

the demodulation process was effective in the case of higher SNR.

3.10 Discussion on the Tradeoff between Radar and Communication Performances

Section 3.7 has demonstrated that the proposed waveform is sufficiently Doppler-tolerant. Furthermore, according to Sect. 2.3, the proposed waveform is capable of increasing the transmission rate in communication use by assigning more communication subcarriers. Nevertheless, there is a trade-off between the Doppler tolerance and the transmission rate. In order to make it clear, this section examines the radar performance when doubling the transmission rate, that is, the number of communication subcarriers from 4 to 8.

Here, there would be two ways to double the transmission rate. One is to assign 4 extra communication subcarriers outside the radar modulation bandwidth β if it is possible to accommodate them within a guard band or regulation band, which is referred to as "Out-Band" herein. The other is to assign 4 extra communication subcarriers inside the radar modulation bandwidth, which is referred to as "In- and Out-Band" herein. In the case of "Out-Band", the communication subcarriers were assigned at the 19th, 20th, 28th, and 29th subcarriers in addition to the 17th, 18th, 30th, and 31st subcarriers in Fig. 7. On the other hand, in the case of "In- and Out-Band", communication subcarriers were added at the 0th, 1st, 15th, and 16th subcarriers.

Figure 19 shows the probability of radar signal detection when doubling the number of communication subcarriers with $\eta = -20$ dB, wherein fast-moving targets with a Doppler frequency of $0.1 f_s$ are assumed to be detected. As can be seen, a slightly higher SNR is needed in any case of 8 subcarriers compared to that of 4 subcarriers. That means that the proposed waveform becomes less Doppler-tolerant when increasing communication subcarriers. In addition, Fig. 19 also shows the probability of detection in the case

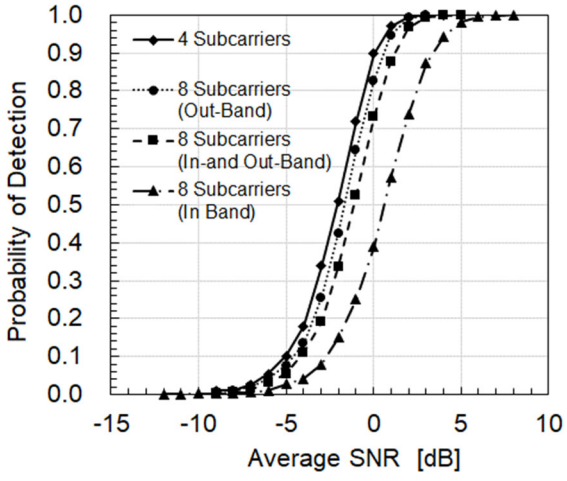

Fig. 19 The probability of radar signal detection for fast-moving targets with $f_d = 0.1 f_s$ when doubling the number of communication subcarriers ($\eta = -20$ dB).

that all the communication subcarriers are assigned inside the radar modulation bandwidth, which is referred to as "In-Band". From these results, it is concluded that the proposed waveform becomes less Doppler-tolerant when assigning more communication subcarriers inside the radar modulation bandwidth. Therefore, it is necessary to maintain the range-Doppler coupling of the original LFM as much as possible in order to be Doppler-tolerant, as discussed in Sect. 3.7. That can be also predicted by analyzing the ambiguity function as shown in Appendix D.

In practice, it is important to design the number of communication subcarriers, balancing the Doppler tolerance and the transmission rate.

4. Conclusions

This study has proposed a Doppler-tolerant waveform and a modulation/demodulation scheme for joint radar and communication systems. In the proposed waveform, communication symbols are embedded in the sideband of an LFM pulse based on the OFDM scheme. The numerical simulations have successfully demonstrated that our waveform is sufficiently Doppler-tolerant to detect fast-moving targets such as aircraft, and the modulation/demodulation scheme was effective for joint radar and communication systems.

In addition, we have discussed the trade-off between the Doppler tolerance and the transmission rate in the proposed waveform and clarified that it is important in practice to balance the Doppler tolerance and the transmission rate to be needed.

However, the proposed waveform has two disadvantages to be solved in the future. One is that the waveform's envelope within a pulse is not constant. This implies that the proposed waveform reduces the SNR of the radar signal in comparison with an LFM pulse if the transmitting peak powers are equal. Therefore, the PAPR should be reduced with some approaches, such as those of [67]–[69]. The other disadvantage is that the transmitted signals fluctuate per pulse, depending on the embedded communication symbols. This causes the range sidelobes to fluctuate per pulse. Therefore, the range sidelobes should be equalized with some approach like [50], [70] to suppress clutter using conventional techniques such as a moving target indicator. These disadvantages will be addressed in future studies.

References

[1] H.T. Hayvaci and B. Tavli, "Spectrum sharing in radar and wireless communication systems: A review," 2014 International Conference on Electromagnetics in Advanced Applications (ICEAA), pp.810–813, 2014.
[2] C. Baylis, M. Fellows, L. Cohen, and R.J. Marks, II, "Solving the spectrum crisis," IEEE Microw. Mag., vol.15, no.5, pp.94–107, July/Aug. 2014.
[3] H. Griffiths, L. Cohen, S. Watts, E. Mokole, C. Baker, M. Wicks, and S. Blunt, "Radar spectrum engineering and management: Technical and regulatory issues," Proc. IEEE, vol.103, no.1, pp.85–102, Jan. 2015.
[4] L. Han and K. Wu, "Joint wireless communication and radar sensing systems — State of the art and future prospects," IET Microw. Antennas Propag., 2013, vol.7, no.11, pp.876–885, 2013.
[5] A. Hassanien, M.G. Amin, Y.D. Zhang, and F. Ahmad, "Signaling strategies for dual-function radar communications: An overview," IEEE Aerosp. Electron. Syst. Mag., vol.31, no.10, pp.36–45, Oct. 2016.
[6] K. Uchiyama and R. Kohno, "Inter-vehicle spread spectrum communication and ranging system with interference canceller," 1999 IEEE/IEEJ/JSAI International Conference on Intelligent Transportation Systems, pp.778–782, 1999.
[7] K. Mizutani and R. Kohno, "Inter-vehicle spread spectrum communication and ranging system with concatenated EOE sequence," IEEE Trans. Intell. Transp. Syst., vol.2, no.4, pp.180–191, Dec. 2001.
[8] A. Ueda and K. Mizui, "Vehicle-to-vehicle communication and ranging system using code-hopping spread spectrum technique with code collision avoidance algorithm," Proc. 2002 IEEE Canadian Conference on Electrical and Computer Engineering, pp.1250–1254, 2002.
[9] S. Lindenmeier, K. Boehm, and J.F. Luy, "A wireless data link for mobile applications," IEEE Microw. Wireless Compon. Lett., vol.13, no.8, pp.326–328, Aug. 2003.
[10] S.J. Xu, Y. Chen, and P. Zhang, "Integrated radar and communication based on DS-UWB," Proc. 2006 Ultrawideband and Ultrashort Impulse Signals, pp.142–144, 2006.
[11] H. Zhang, L. Li, and K. Wu, "24 GHz software-defined radar system for automotive applications," Proc. 10th European Conference on Wireless Technology, pp.138–141, 2007.
[12] M. Jamil, H.-J. Zepernick, and M.I. Pettersson, "On integrated radar and communication systems using oppermann sequences," 2008 IEEE Military Communications Conference (MILCOM 2008), 2008.
[13] P. Kumari, J. Choi, N. González-Prelcic, and R.W. Heath, Jr., "IEEE 802.11ad-based radar: An approach to joint vehicular communication-radar system," IEEE Trans. Veh. Technol., vol.67, no.4, pp.3012–3027, April 2018.
[14] G.E.A. Franken, H. Nikookar, and P. van Genderen, "Doppler tolerance of OFDM-coded radar signals," Proc. 3rd European Radar Conference, pp.108–111, 2006.
[15] D. Garmatyuk, J. Schuerger, Y.T. Morton, K. Binns, M. Durbin, and J. Kimani, "Feasibility study of a multi-carrier dual-use imaging radar and communication system," Proc. 4th European Radar Conference, pp.194–197, 2007.
[16] C. Sturm, T. Zwick, and W. Wiesbeck, "An OFDM system concept for joint radar and communications operations," VTC Spring 2009 - IEEE 69th Vehicular Technology Conference, 2009.
[17] D. Garmatyuk, J. Schuerger, K. Kauffman, and S. Spalding, "Wideband OFDM system for radar and communication," 2009 IEEE Radar Conference, 2009.
[18] M. Braun, C. Sturm, A. Niethammer, and F.K. Jondral, "Parametrization of joint OFDM-based radar and communication systems for vehicular applications," 2009 IEEE 20th International Symposium on Personal, Indoor and Mobile Radio Communications, pp.3020–3024, 2009.
[19] P. van Genderen, "A communication waveform for radar," 2010 8th International Conference on Communications, pp.289–292, 2010.
[20] D. Garmatyuk, J. Schuerger, and K. Kauffman, "Multifunctional software-defined radar sensor and data communication system," IEEE Sensors J., vol.11, no.1, pp.99–106, Jan. 2011.
[21] C. Sturm and W. Wiesbeck, "Waveform design and signal processing aspects for fusion of wireless communications and radar sensing," Proc. IEEE, vol.99, no.7, pp.1236–1259, July 2011.
[22] Y.L. Sit, C. Sturm, and T. Zwick, "Doppler estimation in an OFDM joint radar and communication system," Proc. 6th German Microwave Conference, 2011.
[23] S. Gogineni, M. Rangaswamy, and A. Nehorai, "Multi-modal

OFDM waveform design," 2013 IEEE Radar Conference, 2013.
[24] L. Hu, Z. Du, and G. Xue, "Radar-communication integration based on OFDM signal," 2014 IEEE International Conference on Signal Processing, Communications and Computing (ICSPCC), pp.442–445, 2014.
[25] J.R. Krier, M.C. Norko, J.T. Reed, R.J. Baxley, A.D. Lanterman, X. Ma, and J.R. Barry, "Performance bounds for an OFDM-based joint radar and communications system," 2015 IEEE Military Communications Conference (MILCOM 2015), pp.511–516, 2015.
[26] J. Ellinger, Z. Zhang, M. Wicks, and Z. Wu, "Multi-carrier radar waveforms for communications and detection," IET Radar, Sonar Navig., vol.11, no.3, pp.444–452, 2017.
[27] Y. Liu, G. Liao, J. Xu, Z. Yang, and Y. Zhang, "Adaptive OFDM integrated radar and communications waveform design based on information theory," IEEE Commun. Lett., vol.21, no.10, pp.2174–2177, Oct. 2017.
[28] X. Tian and Z. Song, "On radar and communication integrated system using OFDM signal," 2017 IEEE Radar Conference (RadarConf), pp.318–323, 2017.
[29] S.H. Dokhanchi, M.R.B. Shankar, T. Stifter, and B. Ottersten, "OFDM-based automotive joint radar-communication system," 2018 IEEE Radar Conference (RadarConf18), pp.902–907, 2018.
[30] C.D. Ozkaptan, E. Ekici, O. Altintas, and C.-H. Wang, "OFDM pilot-based radar for joint vehicular communication and radar systems," 2018 IEEE Vehicular Networking Conference (VNC), 2018.
[31] E. BouDaher, A. Hassanien, E. Aboutanios, and M.G. Amin, "Towards a dual-function MIMO radar-communication system," 2016 IEEE Radar Conference (RadarConf), 2016.
[32] A. Hassanien, M.G. Amin, Y.D. Zhang, and B. Himed, "A dual-function MIMO radar-communications system using PSK," 2016 24th European Signal Processing Conference (EUSIPCO), pp.1613–1617, 2016.
[33] Z. Geng, R. Xu, H. Deng, and B. Himed, "Fusion of radar sensing and wireless communications by embedding communication signals into the radar transmit waveform," IET Radar, Sonar Navig., vol.12, no.6, pp.632–640, 2018.
[34] Z. Lin and P. Wei, "Pulse amplitude modulation direct sequence ultra wideband sharing signal for communication and radar systems," 2006 7th International Symposium on Antennas, Propagation & EM Theory, 2006.
[35] P. Barrenechea, F. Elferink, and J. Janssen, "FMCW radar with broadband communication capability," Proc. 4th European Radar Conference, pp.130–133, 2007.
[36] Z. Liu, We. Zhang, and S. Xu, "Implementation on the integrated waveform of radar and communication," 2013 International Conference on Communications, Circuits and Systems (ICCCAS), pp.200–204, 2013.
[37] H. Lou, Q. Zhang, B.-S. Liang, and Y.-A. Chen, "Waveform design and analysis for radar and communication integration system," 2015 IET International Radar Conference, 2015.
[38] Y. Xie, R. Tao, and T. Wang, "Method of waveform design for radar and communication integrated system based on CSS," 2011 International Conference on Instrumentation, Measurement, Computer, Communication and Control, pp.737–739, 2011.
[39] Y. Zhang, Q. Li, L. Huang, and J. Song, "Waveform design for joint radar-communication system with multi-user based on MIMO radar," 2017 IEEE Radar Conference (RadarConf), pp.415–418, 2017.
[40] Z. Lin and P. Wei, "Pulse position modulation time hopping ultra wideband sharing signal for radar and communication system," 2006 CIE International Conference on Radar, 2006.
[41] M. Bocquet, C. Loyez, C. Lethien, N. Deparis, M. Heddebaut, A. Rivenq, and N. Rolland, "A multifunctional 60-GHz system for automotive applications with communication and positioning abilities based on time reversal," Proc. 7th European Radar Conference, pp.61–64, 2010.
[42] Y. Nijsure, Y. Chen, S. Boussakta, C. Yuen, Y.H. Chew, and Z. Ding, "Novel system architecture and waveform design for cognitive radar radio networks," IEEE Trans. Veh. Technol., vol.61, no.8, pp.3630–3642, Oct. 2012.
[43] M. Roberton and E.R. Brown, "Integrated radar and communications based on chirped spread spectrum techniques," 2003 IEEE MTTS-Digest, pp.611–614, 2003.
[44] G.N. Saddik, R.S. Singh, and E.R. Brown, "Ultra-wideband multifunctional communications/radar system," IEEE Trans. Microw. Theory Techn., vol.55, no.7, pp.1431–1437, July 2007.
[45] X. Chen, X. Wang, S. Xu, and J. Zhang, "A novel radar waveform compatible with communication," 2011 International Conference on Computational Problem-Solving (ICCP), pp.177–18, 2011.
[46] Z. Zhao and D. Jiang, "A novel integrated radar and communication waveform based on LFM signal," 2015 IEEE 5th International Conference on Electronics Information and Emergency Communication, pp.219–223, 2015.
[47] M.J. Nowak, M. Wicks, and Z. Zhang, "Co-designed radar-communication using linear frequency modulation waveform," IEEE Aerosp. Electron. Syst. Mag., vol.31, no.10, pp.28–35, Oct. 2016.
[48] R.-Q. Huang, X.-L. Zhao, Q. Zhang, and J. Jia, "Spectrum extension research of radar-communication integrated waveform," 2016 2nd IEEE International Conference on Computer and Communications, pp.1804–1808, 2016.
[49] M.J. Nowak, Z. Zhang, L. LoMonte, M. Wicks, and Z. Wu, "Mixed-modulated linear frequency modulated radar-communications," IET Radar, Sonar Navig., vol.11, no.2, pp.313–320, 2017.
[50] C. Sahin, J.G. Metcalf, and S.D. Blunt, "Filter design to address range sidelobe modulation in transmit-encoded radar-embedded," 2017 IEEE Radar Conference (RadarConf), pp.1509–1514, 2017.
[51] Y. Zhang, Q. Li, L. Huang, C. Pan, and J. Song, "A modified waveform design for radar-communication integration based on LFM-CPM," 2017 IEEE 85th Vehicular Technology Conference (VTC Spring), 2017.
[52] I.P. Eedara, A. Hassanien, M.G. Amin, and B.D. Rigling, "Ambiguity function analysis for dual-function radar communications using PSK signaling," 2018 52nd Asilomar Conference on Signals, Systems, and Computers, pp.900–904, 2018.
[53] H. Men, Z. Song, H. Wen, and G. Liao, "A novel integrated waveform for the radar-communication integration system," 2018 18th IEEE International Conference on Communication Technology, pp.369–375, 2018.
[54] S.D. Blunt and P. Yantham, "Waveform design for radar-embedded communications," 2007 International Waveform Diversity and Design Conference, pp.214–218, 2007.
[55] S.D. Blunt, P., Yatham, and J. Stiles, "Intrapulse radar-embedded communications," IEEE Trans. Aerosp. Electron. Syst., vol.46, no.3, pp.1185–1200, July 2010.
[56] J.G. Metcalf, C. Sahin, S.D. Blunt, and M. Rangaswamy, "Analysis of symbol-design strategies for intrapulse radar-embedded communications," IEEE Trans. Aerosp. Electron. Syst., vol.51, no.4, pp.2914–2931, Oct. 2015.
[57] D. Ciuonzo, A. De Maio, G. Foglia, and M. Piezzo, "Intrapulse radar-embedded communications via multiobjective optimization," IEEE Trans. Aerosp. Electron. Syst., vol.51, no.4, pp.2960–2974, Oct. 2015.
[58] B. Li, J. Lei, W. Cao, L. Wen, and Y. Mou, "Waveform design for radar-embedded communications exploiting spread spectrum technology," IET Commun., vol.10, no.13, pp.1631–1639, 2016.
[59] C. Sahin, J. Jakabosky, P.M. McCormick, J.G. Metcalf, and S.D. Blunt, "A novel approach for embedding communication symbols into physical radar waveforms," 2017 IEEE Radar Conference (RadarConf), pp.1498–1503, 2017.
[60] Y. Gu, L. Zhang, Y. Zhou, and Q. Zhang, "Embedding communication symbols into radar waveform with orthogonal FM scheme," IEEE Sensors J., vol.18, no.21, pp.8709–8719, Nov. 2018.
[61] M.A. Richards, Fundamentals of Radar Signal Processing Second

Edition, McGraw-Hill Education, 2014.
[62] M.A. Richards, J.A. Scheer, and W.A. Holm, Principles of Modern Radar, vol.I: Basic Principles, SciTech Publishing, Raleigh, NC, 2010.
[63] N. Levanon, "Multifrequency complementary phase-coded radar signal," IEE Proc., Radar, Sonar Navig., vol.147, no.6, pp.276–284, Dec. 2000.
[64] T. Takahashi, Y. Kato, K. Isoda, Y. Kitsukawa, and M. Mitsumoto, "A study on waveform design for joint radar and communication systems," IEICE Technical Report, AP2018-47, 2018 (in Japanese).
[65] T. Takahashi, Y. Kato, K. Isoda, Y. Kitsukawa, and M. Mitsumoto, "A novel waveform for joint radar and communication systems," 2019 International Symposium on Antennas and Propagation (ISAP), 2019.
[66] J.G. Proakis and M. Salehi, Digital Communications, 5th ed., McGraw-Hill, New York, 2008.
[67] T. Jiang and Y. Wu, "An overview: Peak-to-average power ratio reduction techniques for OFDM signals," IEEE Trans. Broadcast., vol.54, no.2, pp.257–268, June 2008.
[68] D.-W. Lim, S.-J. Heo, and J.-S. No, "An overview of peak-to-average power ratio reduction schemes for OFDM signals," J. Commun. Netw., vol.11, no, 3, pp.229–239, June 2009.
[69] Y. Rahmatallah and S. Mohan, "Peak-to-average power ratio reduction in OFDM systems: A survey and taxonomy," IEEE Commun. Surveys Tuts., vol.15, no.4, pp.1567–1592, Fourth Quarter 2013.
[70] S.D. Blunt, M.R. Cook, and J. Stiles, "Embedding information into radar emissions via waveform implementation," 2010 International Waveform Diversity and Design Conference, 2010.

Appendix A: Approximate PAPR Distribution

Based on the discussion in Sect. 2.7, the communication subcarrier power would be minor compared with the total power, and (21) would also be small. In this case, the modified Bessel function of the 0-th order can be approximated as in [66]:

$$I_0(x) \approx \frac{e^x}{\sqrt{2\pi x}} \quad (x \gg 1). \tag{A·1}$$

Substituting (A·1) into (22) yields:

$$p(\chi) \approx \frac{1}{2\sqrt{2\pi}\sigma}\left(A\chi^{\frac{1}{2}}\right)^{-\frac{1}{2}} e^{-\frac{(\sqrt{\chi}-A)^2}{2\sigma^2}}. \tag{A·2}$$

Because the PAPR discussion addresses the case of $\chi \gg A_2$, the lower bound of (A·2) becomes:

$$p(\chi) > \frac{1}{2\sqrt{2\pi}\sigma}\chi^{-\frac{1}{2}} e^{-\frac{(\sqrt{\chi}-A)^2}{2\sigma^2}}. \tag{A·3}$$

From (A·3), the upper bound of the probability for $\chi < \chi_p$ at a sampling point is given by:

$$\begin{aligned} P\left[\chi < \chi_p\right] &< 1 - \int_{\chi_p}^{\infty} \frac{1}{2\sqrt{2\pi}\sigma}\chi^{-\frac{1}{2}} e^{-\frac{(\sqrt{\chi}-A)^2}{2\sigma^2}} d\chi \\ &= 1 - Q\left(\frac{\sqrt{\chi_p}-A}{\sigma}\right). \end{aligned} \tag{A·4}$$

Because $\chi \gg A_2$ and $\sigma \ll 1$, the Q function in (A·4) can be approximated as [66]:

$$Q(x) \approx \frac{1}{x\sqrt{2\pi}} e^{-\frac{x^2}{2}} \quad (x \gg 1). \tag{A·5}$$

Substituting (A·5) into (A·4) yields:

$$P\left[\chi < \chi_p\right] < 1 - \frac{\sigma}{\sqrt{2\pi}\left(\sqrt{\chi_p}-A\right)} e^{-\frac{(\sqrt{\chi_p}-A)^2}{2\sigma^2}}. \tag{A·6}$$

Finally, the upper bound for the CDF of the PAPR can be obtained as (29).

Appendix B: Discussion on the Accuracy of the Estimated Doppler Frequency

To extract the communication symbols in asynchronous receivers, the Doppler frequency must be accurately estimated and compensated. Here, we theoretically investigate the accuracy of the estimated Doppler frequency.

The frequency resolution Δf_d in the Doppler spectrum is given by (43), which can be rearranged by introducing the transmit duty factor δ as [61]:

$$\Delta f_d = \frac{\delta}{N_p\tau} = \frac{\delta}{N_p}\Delta f \ll \Delta f. \tag{A·7}$$

That is, the frequency resolution is significantly smaller than the subcarrier interval Δf.

Moreover, the Cramer-Rao lower bound (CRLB) gives the lower bound of the variance of the estimated Doppler frequency as [61]:

$$\sigma_{f_d}^2 \geq \frac{6(\Delta f_d)^2}{(2\pi)^2 N_p SNR_{rad}}, \tag{A·8}$$

where SNR_{rad} is given by (14) or (15). According to (17), SNR_{rad} is much larger than SNR_{com}. Since SNR_{com} in communication receivers should be large enough to detect the communication symbols, SNR_{rad} in communication receivers should be huge. As a result, we can conclude that:

$$\sigma_{f_d}^2 \ll (\Delta f_d)^2 \ll (\Delta f)^2. \tag{A·9}$$

According to (A·9), the estimated Doppler frequency in communication receivers is expected to be accurate, which is significantly less than the frequency resolution and the subcarrier interval.

Appendix C: Discussion on the Accuracy of the Estimated Delay Time

To extract the communication symbols in asynchronous receivers, the delay time must also be accurately estimated and compensated. Here, we theoretically investigate the accuracy of the estimated delay time.

The major error factors for the estimated delay time are the range-Doppler coupling and noise. The first factor is inevitable in our waveform. According to (41), the accuracy of the estimated delay time due to range-Doppler coupling is dependent on the accuracy of the estimated Doppler frequency. As discussed in Appendix B, the accuracy of the

estimated Doppler frequency depends on the frequency resolution of the Doppler spectrum. Therefore, the error of the estimated delay time due to range-Doppler coupling can be quantified as:

$$\Delta t = \frac{\tau \Delta f_d}{\beta} = \frac{\Delta f_d}{\beta \Delta f}. \tag{A· 10}$$

Considering (A· 7), therefore, it can be concluded that:

$$\Delta t \ll \frac{1}{\beta}. \tag{A· 11}$$

Because the right-hand side of (A· 11) is the range resolution, the error in the estimated delay time due to range-Doppler coupling is much smaller than the range resolution.

Next, the second error factor, i.e., noise is considered. The CRLB also gives the lower bound of the variance of the estimated delay time as [61]:

$$\sigma_{\Delta t}^2 \geq \frac{1}{8\pi^2 SNR_{rad} B_{rms}^2}, \tag{A· 12}$$

where B_{rms} is the root-mean-square value of the bandwidth. In the LFM pulse, B_{rms} is given by [61]:

$$B_{rms} = \frac{\beta}{\sqrt{12}}. \tag{A· 13}$$

Substituting (A· 13) into (A· 12) yields:

$$\sigma_{\Delta t}^2 \geq \frac{3}{2\pi^2 SNR_{rad} \beta^2}. \tag{A· 14}$$

Because SNR_{rad} in communication receivers is sufficiently large to detect the radar signal, it can be concluded that:

$$\sigma_{\Delta t}^2 \ll \frac{1}{\beta^2}. \tag{A· 15}$$

This means that the variance of the estimated delay time is also notably smaller than the range resolution. In conclusion, the delay time estimation is expected to be accurate and significantly less than the range resolution.

Appendix D: Ambiguity Functions of the Proposed Wave form with 8 Communication Subcarriers

Figures A· 1(a), A· 1(b), and A· 1(c) show typical ambiguity functions of the proposed waveform with 8 communication subcarriers of $\eta = -20$ dB. As can be seen, the range-Doppler coupling deteriorates gradually as more communication subcarriers are assigned inside the radar modulation bandwidth.

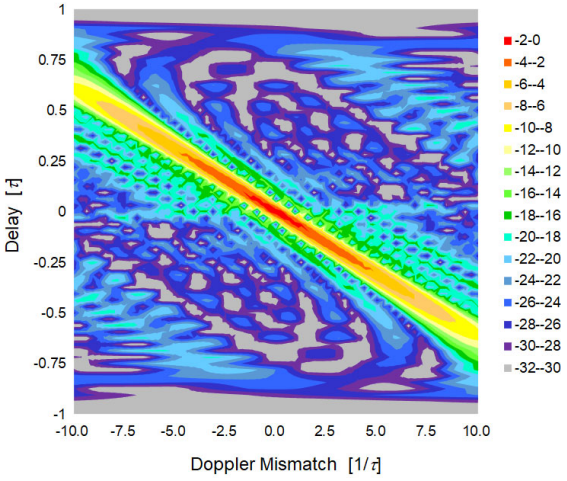

(a) Out-Band

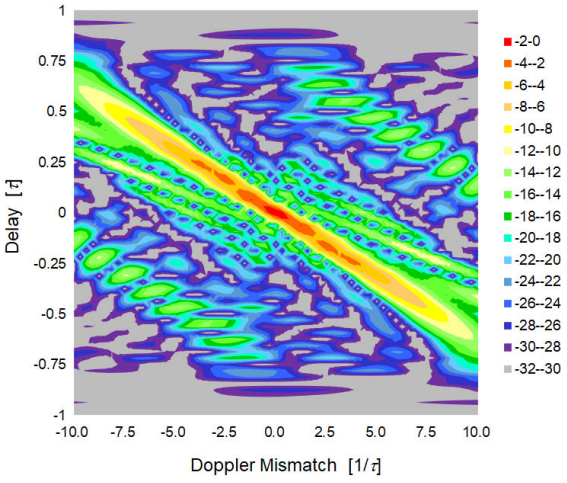

(b) In- and Out-Band

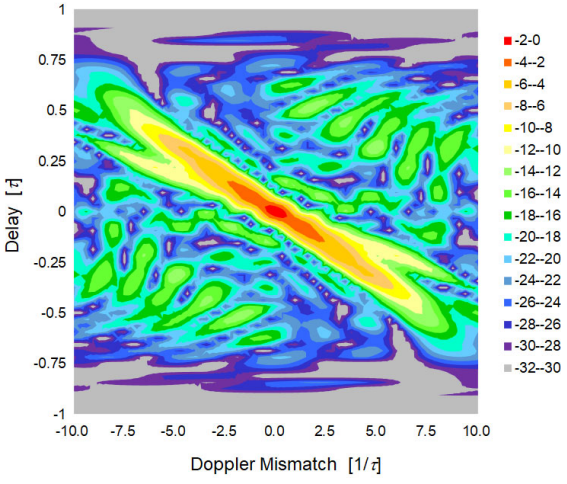

(c) In-Band

Fig. A· 1 Typical ambiguity functions of the proposed waveform with 8 communication subcarriers of $\eta = -20$ dB.

Toru Takahashi was born in Kanagawa, Japan, on January 6, 1970. He received his B.E. and M.E. degrees in electrical engineering from Waseda University, Tokyo, Japan, in 1992 and 1994, respectively, and his D.E. degree from the same university in 2010. In 1994, he joined Mitsubishi Electric Corporation, Japan, where he has been engaged in research and development on antennas and wireless systems such as radar and radio communication. Currently, he is a Manager of Antennas Technology Department, Information Technology R&D Center. He received the Young Engineer Award from the Institute of Electronics, Information and Communication Engineers (IEICE) of Japan in 1999, IEICE Communications Society Best Paper Award in 2013 and 2018. He is a senior member of the IEEE.

Yasunori Kato received his B.E. and M.E. degrees in electrical and electronic system engineering from Saitama University, Japan, in 2000 and 2002, respectively. In 2002, he joined Mitsubishi Electric Corporation, Japan, where he has been engaged in research and development on radio communication systems.

Kentaro Isoda received his B.E. degree from Kyoto University in 2005, and M.I. degree from Graduate School of Informatics, Kyoto University in 2007, respectively. He has been with Mitsubishi Electric Corporation since 2007. His current research interest is in radar signal processing.

Yusuke Kitsukawa was born in Kanagawa, Japan, on May 16, 1980. He received his B.E. degree in electrical engineering from Tokyo University of Science, Tokyo, Japan, in 2003, and his M.E. degree in electronic engineering from Tokyo University, Tokyo, Japan, in 2005. In 2005, he joined Mitsubishi Electric Corporation, Japan, where he has been engaged in research and development on transceivers for radar system. Currently, he is a head researcher of Electromagnetic Platform Technology Department, Information Technology R&D Center. He received the Young Engineer Award from the Institute of Electronics, Information and Communication Engineers (IEICE) of Japan in 2009. He is a member of the IEEE.